

Epidemic evolution model considering individual heterogeneity in multi-layer hypernetwork

Shijie Xie(谢仕杰), Peiwen Wang(王沛文), Zhiping Wang(王志平), Yueyue Zheng(郑月月), and Lin Wang(王琳)
Citation: Chin. Phys. B, 2026, 35 (**3**): 030202. DOI: 10.1088/1674-1056/adf31c
http://cpb.iphy.ac.cn; http://iopscience.iop.org/cpb

What follows is a list of articles you may be interested in

An epidemic model considering multiple factors based on multilayer hypernetworks

Yue-Yue Zheng(郑月月), Zhi-Ping Wang(王志平), Ya-Nan Sun(孙雅楠), Shi-Jie Xie(谢仕杰), and Lin Wang(王琳)
Chin. Phys. B, 2025, 34 (**10**): 100201. DOI: 10.1088/1674-1056/add50c

Finite-time decentralized event-triggered state estimation for coupled neural networks under unreliable Markovian network against mixed cyberattacks

Xiulin Wang(汪修林), Youzhi Cai(蔡有志), and Feng Li(李峰)
Chin. Phys. B, 2024, 33 (**11**): 110207. DOI: 10.1088/1674-1056/ad7e9a

Impact of asymptomatic infected individuals on epidemic transmission dynamics in multiplex networks with partial coupling

Xin Hu(胡鑫), Jiaxing Chen(陈嘉兴), and Chengyi Xia(夏承遗)
Chin. Phys. B, 2024, 33 (**10**): 100202. DOI: 10.1088/1674-1056/ad757b

Impact of different interaction behavior on epidemic spreading in time-dependent social networks

Shuai Huang(黄帅), Jie Chen(陈杰), Meng-Yu Li(李梦玉),Yuan-Hao Xu(徐元昊), and Mao-Bin Hu(胡茂彬)
Chin. Phys. B, 2024, 33 (**3**): 030205. DOI: 10.1088/1674-1056/ad147f

Chaos control in the nonlinear Schrödinger equation with Kerr law nonlinearity

Yin Jiu-Li (殷久利), Zhao Liu-Wei (赵刘威), Tian Li-Xin (田立新)
Chin. Phys. B, 2014, 23 (**2**): 020204. DOI: 10.1088/1674-1056/23/2/020204

Epidemic evolution model considering individual heterogeneity in multi-layer hypernetwork

Shijie Xie(谢仕杰)[1], Peiwen Wang(王沛文)[2], Zhiping Wang(王志平)[1,†], Yueyue Zheng(郑月月)[1], and Lin Wang(王琳)[3,‡]

[1] *School of Science, Dalian Maritime University, Dalian* 116026, *China*
[2] *Department of Surface Ship Command, Dalian Naval Academy, Dalian* 116001, *China*
[3] *Department of Respiratory and Critical Care Medicine, Institute of Respiratory Diseases, The First Affiliated Hospital of Dalian Medical University, Dalian* 116011, *China*

(Received 16 June 2025; revised manuscript received 16 July 2025; accepted manuscript online 23 July 2025)

In recent years, the dynamic coupling mechanisms between information dissemination and epidemic transmission have garnered significant attention. Existing studies predominantly focus on the impact of individual awareness on disease spread; however, in reality, the factors driving awareness shifts and heterogeneous perceptions of epidemics vary substantially among individuals with different health statuses. Moreover, traditional pairwise interaction networks fail to capture the complexity of social contagion processes. To address these gaps, this study proposes a three-layer hypernetwork epidemic model (mass media layer–information layer–epidemic layer) based on evolutionary hypergraphs, incorporating individual heterogeneity and higher-order group interactions. The information layer employs an asthenic awareness–powerful awareness–asthenic awareness (APA) propagation model to characterize the diffusion of epidemic awareness, integrated with a perceived pain level metric to quantify dynamic awareness states among infected individuals. The underlying susceptible–infected–recovered (SIR) model incorporates dual modulation factors that adjust infection and transmission probabilities based on awareness-dependent behaviors. Model validity is verified through microscopic Markov chain approach (MMCA) numerical simulations, which identify epidemic thresholds and analyze key parameters. The key findings reveal that susceptibility and transmission rates are critical factors determining epidemic scale; high-coverage official media can rapidly disseminate accurate information and curb rumors; controlling pain levels and improving recovery efficiency are crucial for reducing the infection peak and shortening epidemic duration. This study provides a systematic analytical framework for understanding the interaction mechanisms among mass media, individual cognition, and epidemic transmission in real-world scenarios.

Keywords: epidemic transmission, information transmission, individual consciousness, multilayer hypernetwork, microscopic Markov chain

PACS: 02.50.Ga, 02.60.Cb, 02.50.Ey

DOI: 10.1088/1674-1056/adf31c **CSTR:** 32038.14.CPB.adf31c

1. Introduction

In the era of globalization, the outbreak of infectious diseases has become an unprecedented threat to human society. Pathogens can spread rapidly across countries, causing significant health, economic and social risks. The COVID-19 pandemic that began at the end of 2019 represents the most serious public health crisis of the 21st century, resulting in a large number of infections and substantial loss of life worldwide. How to characterize the dynamics of epidemic spread within a population has long been a central concern for researchers. Understanding the epidemiological characteristics related to outbreak thresholds and transmission scales is crucial for formulating effective prevention and control strategies.

The process of epidemic spread is usually accompanied by the dissemination of related information, which propagates rapidly through public media,[1–3] thereby reshaping the public's perception of the epidemic. Individuals obtain varying amounts of disease-related information from social media platforms. Such information not only influences their behavioral decisions but also ultimately affects disease transmission.[4,5] Understanding and predicting the interaction between online information dissemination and epidemic spread remains a major challenge in network theory and is of great significance to the social sciences.

In recent years, multilayer networks have been widely adopted as the fundamental framework for investigating the dynamic interaction between information dissemination and epidemic transmission.[6–8] Granell *et al.*[9] proposed the unaware–aware–unaware (UAU) susceptible–infected–susceptible (SIS) model on multiplex networks and identified sub-critical points that can be regulated through awareness diffusion. Subsequently, they extended their research to incorporate self-awareness and media influence, revealing that the sub-critical points associated with social media disappeared.[10] Xia *et al.*[11] investigated the influence of

†Corresponding author. E-mail: wzp@dlmu.edu.cn
‡Corresponding author. E-mail: 1015132938@qq.com

© 2026 Chinese Physical Society and IOP Publishing Ltd. All rights, including for text and data mining, AI training, and similar technologies, are reserved.

mass media on epidemic spreading in two-layer networks and derived epidemic thresholds associated with the interplay between transmission dynamics and network topology. Sun *et al.*[12] introduced three mechanisms of individual awareness generation in multiplex networks and demonstrated that enhanced self-awareness among infected individuals not only reduces epidemic prevalence but also elevates the epidemic threshold.

Previous studies often assumed that all individuals in a network possess identical attributes; however, in reality, each individual is unique. Responses vary across different contexts and health conditions. Therefore, further research is essential to better understand the impact of individual heterogeneity on epidemic spreading in multilayer networks.

Fang *et al.*[13] proposed two opposing viewpoints at the awareness level, supporting physical distancing and anti-distancing behaviors, respectively, and found that awareness enhancement mechanisms help reduce overall epidemic prevalence. Han *et al.*[14] proposed a three-layer network epidemic model consisting of a mass media layer, an information layer (UA_1A_2), and an epidemic layer following the SIS model. Their results showed that increasing the dissemination of negative information while suppressing positive information can more effectively control epidemic outbreaks and spread. Yu *et al.*[15] proposed a three-layer model to analyze the co-evolution of information, immunity and epidemics. The findings indicated that competition between positive and negative information can trigger multi-phase transitions; enhancing positive information cognition and timely immunization are key to reducing epidemic scale and improving emergency management. Yin *et al.*[16] developed a three-layer network model to analyze the collaborative dynamics of information dissemination, vaccination and epidemic evolution. Through game theory and the Markov method, they found that controlling the cost of negative information and improving vaccine efficacy are more effective strategies, whereas excessive investment is unnecessary. Herd behavior may exacerbate epidemic spread, providing a new perspective for understanding transmission dynamics. Meanwhile, although the awareness–powerful awareness–asthenic awareness (APA)-SIS model proposed by Xu *et al.*[17] considered the influence of health status on awareness transformation and deepened the understanding of multilevel communication dynamics, it still had several limitations: it did not incorporate the role of official media in awareness evolution; it did not examine the impact of awareness states on infection rates; it overlooked post-recovery immunity; and it failed to transcend traditional pairwise interaction assumptions, making it difficult to accurately describe complex information diffusion processes in social-media-dominated network topologies with multi-node cooperative propagation.

Hypernetworks, with their multi-node connectivity and hierarchical nesting characteristics, provide powerful mathematical tools for depicting complex real-world propagation pathways. Wang *et al.*[18] proposed two evolution mechanisms for hypernetwork models: hyperedge growth and preferential hyperedge attachment. In 2018, Guo *et al.*[19] extended the evolution process to include three mechanisms: addition of new nodes, connection of existing nodes and link rewiring. In 2020, Wang *et al.*[20] constructed a dynamic hypernetwork-based social network model and demonstrated that the hyperdegree distribution follows a power-law form. Sun *et al.*[21] proposed a susceptible–exposed–infectious–recovered (SEIR) model of dynamic information transmission in social networks from a hypernetwork perspective, incorporating both positive and negative interference effects. By integrating hypernetwork theory with propagation dynamics equations, they introduced an information disturbance function to formulate the dynamic equation of information diffusion. Xie *et al.*[22] proposed a dual-layer weighted dynamic evolution network model from a hypernetwork perspective, incorporating a heterogeneous rewiring rate proportional to connection strength, and found that rewiring behavior significantly affects epidemic control. However, in existing multilayer hypernetwork studies, infection-related information of infected individuals is often assumed to be fully known, neglecting the influence of health status on awareness transformation. In particular, systematic research is lacking on how to quantitatively characterize the dynamic feedback between clinical symptoms and risk perception.

Motivated by these gaps, this paper constructs a three-layer hypernetwork coupling model integrating the mass media layer, the awareness dissemination layer and the infectious disease layer, achieving advances in three key dimensions.

First, in terms of structural characterization, the model captures multidimensional coupling relationships among the mass media layer, information diffusion layer and infectious disease layer, overcoming the limitations of traditional dyadic networks that only describe pairwise interactions. Specifically, in the mass media layer, individuals' exposure to official media information is incorporated and linked to the information diffusion layer; in the information diffusion layer, the APA model is adopted to classify individuals into different awareness states, and hyperdegree is used to represent the proportion of neighbors with strong awareness, thereby determining awareness transition probabilities; for infected individuals, a suffering degree is introduced to characterize awareness evolution. In the infectious disease layer, the susceptible–infected–recovered (SIR) model is employed to describe epidemic dynamics, incorporating two regulatory factors that modulate in-

fection and transmission probabilities; additionally, a normal distribution is used to represent recovery rates, reflecting natural variability in individual recovery speeds and enhancing model realism. Second, regarding the dynamic mechanism, a "pain–consciousness response function" is defined to quantify symptom severity of infected individuals as the core regulator of awareness states. Finally, from an analytical perspective, a multilayer approximation framework based on microscopic Markov chain analysis is developed to investigate the influence of key dynamic parameters on coupled awareness–epidemic dynamics. This framework fills the research gap in hypernetwork propagation dynamics driven by health states and provides a novel theoretical basis for understanding the complex interactions among media intervention, collective awareness and disease transmission. The proposed three-layer coupling model offers an innovative paradigm for exploring epidemic transmission mechanisms and media effects.

The main contributions of this paper are summarized as follows:

(i) A M-APA-SIR three-layer hypernetwork propagation model is proposed, incorporating the influence of mass media on awareness states during infectious disease transmission. Individuals with different awareness states experience different infection risks.

(ii) Considering the interaction between the transmission rate of infected individuals and the infection susceptibility of susceptible individuals facilitates more effective epidemic control.

(iii) Numerical simulations validate the theoretical results derived from the Markov chain analysis, further demonstrating the effectiveness and feasibility of the proposed model and providing reliable strategies for epidemic control.

The remainder of this paper is organized as follows. In Section 2, the proposed epidemic transmission model is described in detail. In Section 3, microscopic Markov chain approach (MMCA) is applied to analyze the model and derive the diffusion threshold. In Section 4, numerical simulations are conducted for further validation and discussion. Finally, Section 5 concludes the paper and outlines future research directions.

2. Description of the model

We first introduce the concept of a hypergraph.

Let $V = \{v_1, v_2, \ldots, v_n\}$ be the finite node set of a hypergraph, and let $E_i = \{v_{i1}, v_{i2}, \ldots, v_{ij}\}$ $(v_{ik} \in V, k \in N^+)$ be a nonempty subset of V. Denote the hyperedge set as $E = \{E_1, E_2, \ldots, E_m\}$, and define the hypergraph as the binary relation $H = (V, E)$. A hypergraph is a generalization of an ordinary graph, in which an edge connects only two vertices; in contrast, a hyperedge can connect an arbitrary number of vertices. The concept of hypergraphs was first proposed by Berge.[23,24] In 2005, Estrada and Rodriguez-Velazquez[25] stated that any network representable by a hypergraph can be regarded as a hypernetwork, and provided a definition of hypernetworks based on hypergraphs.

2.1. Dynamic evolution model

In modern society, information dissemination occurs not only in physical space but also extensively on virtual networks and digital platforms. The interweaving of virtual and real communication channels shapes a complex information diffusion network. In virtual space, users exhibit strong autonomy and randomness: they can join multiple discussion groups simultaneously, forward diverse content and even create new communication hyperedges. Meanwhile, interpersonal contacts in physical settings also influence the scope and pathways of information dissemination. These two channels complement each other, forming a dynamically evolving and heterogeneous network structure that reflects the multimodal propagation mechanism of information in social systems.

Against this background, constructing a network evolution model that captures both large-scale virtual dissemination and real-world interpersonal interactions is of great significance. The dynamic evolution process proposed in this paper simulates real-world information diffusion scenarios by introducing random growth mechanisms of nodes and hyperedges, thereby conforming to the intrinsic characteristics of information flow in society and providing a theoretical foundation for understanding information dissemination in modern complex social networks. The specific evolution mechanism of the model is described as follows.

Considering that individuals with strong social influence are more likely to attract connections, a super-preferential attachment mechanism, as shown in Eq. (1), is adopted for node selection. Here, $h_j(t,t_i)$ denotes the hyperdegree of the jth node in the ith batch at time t, and t_i represents the time at which the ith batch of nodes enters the network

$$H_j(t,t_i) = \frac{h_j(t,t_i)+1}{\sum_{i,j=1} h_j(t,t_i)}. \tag{1}$$

The evolution process of the dynamic network is illustrated in Fig. 1. The overall procedure can be summarized as follows:

(I) Initialization. The initial network consists of N_0 nodes, and each initial hyperedge contains N nodes.

(II) Evolution. New batches of nodes arrive according to a Poisson process $N(t)$ with rate λ'. At each time step, the network evolves according to the following rules.

(i) Add a new node batch with probability p.

When a new batch of $a_{N(t)}$ nodes is introduced at time t, these nodes form hyperedges with $b_{N(t)}$ existing nodes. A to-

tal of m_1 hyperedges are generated, under the constraint that duplicate hyperedges are not allowed. In the ith batch, the probability that the jth node is selected follows $H_j(t,t_i)$.

(ii) Add new hyperedges with probability q.

A node is randomly selected from the network and included in newly created hyperedges. The selected node, together with $b_{N(t)}$ existing nodes, forms a new hyperedge. A total of m_2 hyperedges are constructed, ensuring uniqueness and non-repetition. The selection follows the hyperdegree preferential attachment mechanism defined in Eq. (1).

(iii) Reconnect hyperedges with probability r.

A node and one of its associated hyperedges are randomly selected. The chosen hyperedge is removed, and the node is incorporated into a newly formed hyperedge together with $b_{N(t)}$ reselected existing nodes. This process is repeated m_3 times, ensuring that no duplicate hyperedges are generated. The selection again follows the hyperdegree preferential attachment mechanism defined in Eq. (1).

(III) Repeat. Step (II) is repeated until the network reaches a predefined size.

Here, $a_{N(t)}$ and $b_{N(t)}$ are positive integers drawn from probability density functions $f(a)$ and $g(b)$, respectively, satisfying $(\overline{a} = \int af(a)\,\mathrm{d}a < \infty)$ and $\left(\overline{b} = \int bg(b)\,\mathrm{d}b < \infty\right)$.

The definitions and parameter values used in constructing the initial social network are listed in Table 1. The dynamic evolution process of the hypernetwork is illustrated in Fig. 1.

Table 1. Definitions and parameter values of symbols used in the construction of the initial social network.

Descriptions	Parameters	Value
The number of seed nodes	N_0	35
The rate of new node batches arrivals	λ'	2
Probability density function describing the distribution of the number of nodes per batch	$f(a)$	uniform distribution on (3,7)
Probability density function describing the distribution of the selected existing nodes	$g(b)$	Poisson process with rate 4
Probability of adding new node batches	p	0.3
Probability of adding new hyperedges	q	0.2
Probability of reconnecting hyperedges	r	0.5
The number of new hyperedges formed in process of adding node batches	m_1	uniform distribution on (8,10)
The number of new hyperedges formed in adding new hyperedges	m_2	uniform distribution on (8,10)
The number of new hyperedges formed in reconnecting hyperedges	m_3	uniform distribution on (8,10)

2.2. Three-layer coupled M-APA-SIR model

In this section, we propose a three-layer hypernetwork as a modeling framework to describe the coupled dynamic process. This framework more explicitly captures the subtle differences in how individuals perceive and respond to epidemic information, thereby enhancing our understanding of epidemic transmission associated with awareness dissemination. As shown in Fig. 1, we assume that each node in one layer is mapped one-to-one to the corresponding node in the other layers. That is, the three-layer network shares an identical node set, while each layer exhibits distinct connectivity patterns.

As shown in Fig. 1, the first layer represents the disease-related information network, through which individuals obtain epidemic updates from mass media. The second layer corresponds to the information dissemination layer, where unconscious individuals are not considered. Due to uncertainties in information transmission and heterogeneity in individual acceptance, individuals exhibit different levels of understanding of epidemic-related information. We classify individuals into two categories: those with strong awareness and those with weak awareness. The third layer is the physical contact network of epidemic transmission, referred to as the epidemic layer, which characterizes the regulatory effects of different awareness levels on infection and transmission probabilities.

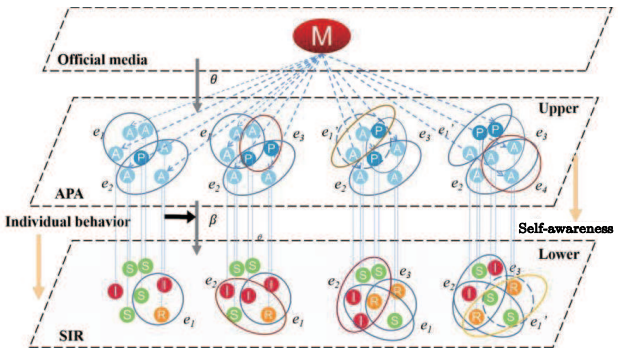


Fig. 1. Schematic illustration of the multilayer structure in the proposed M-APA-SIR model. The top layer (mass media layer) represents the release of official information to the middle layer. The middle virtual contact network shares the same node set as the physical contact network. The middle layer corresponds to the information dissemination layer (APA model), and the bottom layer represents the epidemic transmission layer (SIR model).

In the awareness communication layer, individuals can exist in two states: asthenic awareness (A) and powerful awareness (P). Asthenic awareness (A) refers to individuals with a low level of concern about the epidemic, insufficient cognition and passive behavioral responses. Such individuals exhibit limited awareness, lack motivation to adopt proactive preventive measures and tend to passively receive epidemic-related information. P refers to individuals who pay close attention to the epidemic and possess a more comprehensive

understanding of relevant information. These individuals are inclined to adopt proactive preventive measures, actively seek information and demonstrate a high level of initiative and protective behavior in response to the epidemic.

During the process of awareness transformation, individuals in different health states exhibit distinct driving mechanisms for state transitions. Considering that individuals may also be influenced by conformity effects, we introduce impact factors ω_1 and ω_2 to characterize the influence of conformity on susceptible and recovered individuals, respectively, in their awareness transition probabilities. Compared with recovered individuals who have previously experienced infection, susceptible individuals are more likely to be influenced by powerful-awareness neighbors, thereby changing their awareness state in the communication layer. Therefore, we assume that weak-awareness susceptible individuals (AS) and weak-awareness recovered individuals (AR) transition to strong awareness with probabilities

$$\lambda_i^{\mathrm{AS}} = \lambda^{\omega_1},\ \ \lambda_i^{\mathrm{AR}} = \lambda^{\omega_2},\ \ (\omega_1 < \omega_2), \tag{2}$$

where λ denotes the information acceptance rate. Conversely, strongly aware susceptible and recovered individuals revert to the weak-awareness state with probabilities τ_1 and τ_2, respectively, and we assume that $(\tau_1 < \tau_2)$.

Infected individuals tend to pay closer attention to their physical condition during infection. After receiving epidemic-related information, weak-awareness infected individuals who experience severe symptoms are more likely to transition to strong awareness. Conversely, strongly aware infected individuals with mild symptoms may reduce their concern and shift to a weak-awareness state in the communication layer. To describe this mechanism, we introduce the Heaviside step function $H(x)$, defined as $H(x) = 1$ when $x > 0$ and $H(x) = 0$ otherwise. A parameter v is introduced to represent the severity threshold of symptoms. Larger values of v correspond to more severe symptoms, whereas smaller values indicate mild symptoms that do not significantly attract attention.

Let $i(t)$ denote the symptom severity of an infected individual at time t. When $i(t) > v$, the perceived pain exceeds the threshold, increasing the likelihood that a weak-awareness infected individual transitions to strong awareness. The corresponding transition probability is given by

$$\lambda_i^{\mathrm{AI}} = \lambda H\left[i(t) - v\right]. \tag{3}$$

Strong-awareness infected individuals remain in their current state when symptoms remain severe. Here, $i(t)$ is assumed to follow a normal distribution, namely $G(i(t)) \sim N(\mu_1, \delta_1)$.

Official media play a crucial role in the timely release of epidemic information. Such dissemination increases public attention and enhances risk awareness and preventive consciousness. To model this process, we introduce an official mass media layer connected to the nodes in the virtual communication layer, reflecting the regulatory role of authoritative media in awareness diffusion. Since not all individuals consistently follow news media in reality, we assume that the coverage rate M of official information is limited and generates random mappings between media and nodes in the information dissemination layer. Let $L = (l_1, l_2, \ldots, l_n)$ denote a partial mapping vector. When official media release accurate information, individuals in state A who receive the news transition to state P with probability θ. The transition probability induced by media exposure is defined as

$$\theta_i = \begin{cases} \theta,\ l_i = 1, \\ 0,\ l_i = 0. \end{cases} \tag{4}$$

In the underlying physical contact layer, the SIR model is employed to describe infectious disease transmission. Individuals exist in one of three states: susceptible (S), infected (I) or recovered (R). Susceptible individuals become infected through contact with infected neighbors with probability β, while infected individuals recover with probability γ and transition to the recovered state.

Individuals with weak awareness tend to adopt fewer protective behaviors, whereas those with strong awareness are more likely to implement preventive measures such as mask wearing, medication use and social distancing. These behaviors reduce both susceptibility and transmissibility, thereby mitigating epidemic spread. Accordingly, we introduce influence coefficients φ_1 and φ_2 $(0 < \varphi_1, \varphi_2 < 1)$ to quantify the reduction effects of awareness on infection transmission. For example, a weak-awareness susceptible individual (AS) may be infected by a weak-awareness infected individual (AI) or a strong-awareness infected individual (PI) with probabilities β^{AA} and β^{AP}, respectively. Similarly, infection probabilities for a strong-awareness susceptible individual are denoted by β^{PA} and β^{PP}. The infection rates are defined as

$$\beta^{\mathrm{AA}} = \alpha\beta,\ \ \beta^{\mathrm{AP}} = \alpha\varphi_2\beta,\ \ \beta^{\mathrm{PA}} = \varphi_1\alpha\beta,\ \ \beta^{\mathrm{PP}} = \varphi_1\alpha\varphi_2\beta,$$

where α represents the probability that a susceptible individual is biologically susceptible to viral invasion, and β denotes the transmission probability of an infected individual.

Regarding recovery dynamics, we consider heterogeneity in individual health conditions and recovery capacities. The baseline recovery probability γ_{p} is assumed to follow a normal distribution $G(\gamma_i) \sim N(\mu_2, \delta_2)$, where μ_2 denotes the average recovery capacity of the population and δ_2 represents variability across individuals. Since infected individuals with stronger awareness are more likely to seek timely treatment, we introduce an influence factor ξ $(0 < \xi < 1)$, and define the adjusted recovery probability as $\gamma_{\mathrm{a}} = \xi\gamma_{\mathrm{p}}$.

3. Model theoretical analysis

Based on the dynamic evolution mechanism of hypernetworks introduced in Subsection 2.1, this section employs mean-field theory [26,27] to analyze the hyperdegree distribution of the hypernetwork model. Assume that $h_j(t,t_i)$ is a continuous real variable. The following three dynamic equations for the hyperdegree can then be derived:

$$\frac{\partial h_j(t,t_i)}{\partial t} = pm_1 b\lambda' \frac{h_j(t,t_i)}{\sum_{i,j} h_j(t,t_i)}, \tag{5}$$

$$\frac{\partial h_j(t,t_i)}{\partial t} = qm_2 \left(\frac{1}{N(t)} + b\frac{h_j(t,t_i)}{\sum_{i,j} h_j(t,t_i)} \right), \tag{6}$$

$$\frac{\partial h_j(t,t_i)}{\partial t} = rm_3 \left(-\frac{1}{N(t)} + b\frac{h_j(t,t_i)}{\sum_{i,j} h_j(t,t_i)} \right). \tag{7}$$

Here, $N(t)$ represents the total number of nodes in the hypernetwork at time t, and it is given by $N(t) = p\bar{a}\lambda' t$.

Combining Eqs. (5)–(7), we obtain

$$\frac{\partial h_j(t,t_i)}{\partial t} = pm_1 b\lambda' \frac{h_j(t,t_i)}{\sum_{i,j} h_j(t,t_i)} + (qm_2 + rm_3) b\frac{h_j(t,t_i)}{\sum_{i,j} h_j(t,t_i)} + \frac{qm_2 - rm_3}{N(t)}. \tag{8}$$

By Poisson process theory, we have $E(N(t)) = p\lambda' t$. Let

$$x = \frac{1}{p\lambda' t}\sum_{i,j} h_j(t,t_i), \tag{9}$$

then we obtain

$$\frac{\partial h_j(t,t_i)}{\partial t} = m_1 b\frac{h_j(t,t_i)}{xt} + (qm_2 + rm_3) b\frac{h_j(t,t_i)}{xp\lambda' t} + \frac{qm_2 - rm_3}{p\bar{a}\lambda' t}. \tag{10}$$

Given the initial condition that a node in the ith batch satisfies $h_j(t,t_i) = m_1$ at its generation time, the solution to this equation is

$$h_j(t,t_i) = \left(m_1 + \frac{C}{D}\right)\left(\frac{t}{t_i}\right)^D - \frac{C}{D}, \quad j = 1,2,3,\ldots,a_i. \tag{11}$$

Here

$$C = \frac{qm_2 - rm_3}{p\bar{a}\lambda'}, \quad D = \frac{m_1 b}{x} + \frac{(qm_2 - rm_3)b}{xp\lambda'},$$

and x satisfies the equation

$$x = \frac{1}{p\lambda' t}\int g(b)\,\mathrm{d}b \int \left[\left(m_1 + \frac{B}{A}\right)\left(\frac{t}{t_i}\right)^A - \frac{B}{A}\right]\mathrm{d}t. \tag{12}$$

In the virtual communication layer, if there is a link between nodes v_{ij} and v_{kl}, then $a_{ijkl} = 1$; otherwise, $a_{ijkl} = 0$. In the epidemic transmission layer, if there is a link between nodes v_{ij} and v_{kl}, then $b_{ijkl} = 1$; otherwise, $b_{ijkl} = 0$. Here, v_{ij} represents the jth node in the ith batch, and v_{kl} is defined similarly. Node v_{ij} is in one of the six states at time t with probabilities $P_j^{\mathrm{AS}}(t,t_i)$, $P_j^{\mathrm{PS}}(t,t_i)$, $P_j^{\mathrm{AI}}(t,t_i)$, $P_j^{\mathrm{PI}}(t,t_i)$, $P_j^{\mathrm{AR}}(t,t_i)$, and $P_j^{\mathrm{PR}}(t,t_i)$, respectively. Let $\Theta_j^{\mathrm{AS}}(t,t_i)$, $\Theta_j^{\mathrm{AI}}(t,t_i)$, and $\Theta_j^{\mathrm{AR}}(t,t_i)$ denote the probabilities that weakly – aware individuals in the corresponding states at node j of the ith batch at time t do not transition into strongly – aware individuals. Let $q_j^{\mathrm{AS}}(t,t_i)$ and $q_j^{\mathrm{PS}}(t,t_i)$ denote the probabilities that individuals in the corresponding states at node j of the ith batch at time t avoid infection from their neighbors. Assuming that the transition probabilities of each node are independent, we obtain

$$\begin{cases} \Theta_j^{\mathrm{AS}}(t,t_i) = \prod_k \prod_l \left[1 - a_{ijkl} P_l^{\mathrm{P}}(t,t_k)\,\omega_j(t,t_i)\lambda_j^{\mathrm{AS}}(t,t_i)\right], \\ \Theta_j^{\mathrm{AI}}(t,t_i) = \lambda H[v - i(t)], \\ \Theta_j^{\mathrm{AR}}(t,t_i) = \prod_k \prod_l \left[1 - a_{ijkl} P_l^{\mathrm{P}}(t,t_k)\,\omega_j(t,t_i)\lambda_j^{\mathrm{AR}}(t,t_i)\right], \\ q_j^{\mathrm{AS}}(t,t_i) = \prod_k \prod_l \left[1 - b_{ijkl} P_l^{\mathrm{AI}}(t,t_k)\,\omega_j(t,t_i)\,\beta_j^{\mathrm{AA}}(t,t_i)\right] \\ \qquad \times \left[1 - b_{ijkl} P_l^{\mathrm{PI}}(t,t_k)\,\omega_j(t,t_i)\,\beta_j^{\mathrm{AP}}(t,t_i)\right], \\ q_j^{\mathrm{PS}}(t,t_i) = \prod_k \prod_l \left[1 - b_{ijkl} P_l^{\mathrm{AI}}(t,t_k)\,\omega_j(t,t_i)\,\beta_j^{\mathrm{PA}}(t,t_i)\right] \\ \qquad \times \left[1 - b_{ijkl} P_l^{\mathrm{PI}}(t,t_k)\,\omega_j(t,t_i)\,\beta_j^{\mathrm{PP}}(t,t_i)\right]. \end{cases} \tag{13}$$

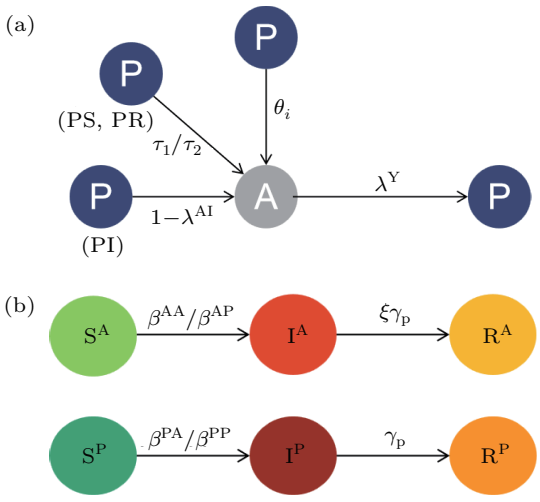


Fig. 2. (a) Represents the probability of consciousness transformation under different infection states and the influence of mass media; (b) represents the transformation probabilities of epidemic states under different states of consciousness.

Considering that individuals with a larger number of neighbors exhibit higher probabilities of receiving information and becoming infected, we employ $\omega_j(t,t_i)$ — an indicator defined based on node hyperdegree — to quantify the relative

abundance of neighbors for node j. This metric characterizes the influence of neighbor quantity on the node's state transition dynamics. Formally, $\omega_j(t,t_i)$ serves as a hyperdegree-based measure that captures how neighborhood size modulates the magnitude of neighbor-induced effects during state evolution

$$\omega_j(t,t_i)=\frac{h_j(t,t_i)}{\mathrm{Max}\left(h(t)\right)}. \tag{14}$$

According to Fig. 2(a) and Eq. (14), a state transition probability tree is constructed to represent the transition probabilities among the six possible states, as shown in Fig. 3.

$$\begin{cases}
P_j^{\mathrm{AS}}(t+1,t_i)=P_j^{\mathrm{AS}}(t,t_i)\,\Theta_j^{\mathrm{AS}}(t,t_i)\,(1-\theta)\,q_j^{\mathrm{AS}}(t,t_i)\\
\quad +P_j^{\mathrm{PS}}(t,t_i)\,\tau_1\,(1-\theta)\,q_j^{\mathrm{AS}}(t,t_i),\\
P_j^{\mathrm{PS}}(t+1,t_i)=P_j^{\mathrm{AS}}(t,t_i)\,q_j^{\mathrm{PS}}(t,t_i)\\
\quad \times\left(1-\Theta_j^{\mathrm{AS}}(t,t_i)+\Theta_j^{\mathrm{AS}}(t,t_i)\,\theta\right)\\
\quad +P_j^{\mathrm{PS}}(t,t_i)\,q_j^{\mathrm{PS}}(t,t_i)\left(1-\tau_1+\tau_1\theta\right),\\
P_j^{\mathrm{AI}}(t+1,t_i)=P_j^{\mathrm{AS}}(t,t_i)\,\Theta_j^{\mathrm{AS}}(t,t_i)\,(1-\theta)\left(1-q_j^{\mathrm{AS}}(t,t_i)\right)\\
\quad +P_j^{\mathrm{PS}}(t,t_i)\,\tau_1\,(1-\theta)\left(1-q_j^{\mathrm{AS}}(t,t_i)\right)\\
\quad +P_j^{\mathrm{AI}}(t,t_i)\,\Theta_j^{\mathrm{AI}}(t,t_i)\,(1-\theta)\,(1-\gamma_{\mathrm{a}})\\
\quad +P_j^{\mathrm{PI}}(t,t_i)\,\Theta_j^{\mathrm{AI}}(t,t_i)\,(1-\theta)\,(1-\gamma_{\mathrm{a}}),\\
P_j^{\mathrm{PI}}(t+1,t_i)=P_j^{\mathrm{AS}}(t,t_i)\,(1-q_j^{\mathrm{PS}}(t,t_i))\\
\quad \times\left(1-\Theta_j^{\mathrm{AS}}(t,t_i)+\Theta_j^{\mathrm{AS}}(t,t_i)\,\theta\right)\\
\quad +P_j^{\mathrm{PS}}(t,t_i)\,(1-q_j^{\mathrm{PS}}(t,t_i))\left(1-\tau_1+\tau_1\theta\right)\\
\quad +P_j^{\mathrm{AI}}(t,t_i)\,(1-\gamma_{\mathrm{p}})\left(1-\Theta_j^{\mathrm{AI}}(t,t_i)+\Theta_j^{\mathrm{AI}}(t,t_i)\,\theta\right)\\
\quad +P_j^{\mathrm{PI}}(t,t_i)\,(1-\gamma_{\mathrm{p}})\left(1-\Theta_j^{\mathrm{AI}}(t,t_i)+\Theta_j^{\mathrm{AI}}(t,t_i)\,\theta\right),\\
P_j^{\mathrm{AR}}(t+1,t_i)=P_j^{\mathrm{AI}}(t,t_i)\,\Theta_j^{\mathrm{AI}}(t,t_i)\,(1-\theta)\,\gamma_{\mathrm{a}}\\
\quad +P_j^{\mathrm{PI}}(t,t_i)\,\Theta_j^{\mathrm{AI}}(t,t_i)\,(1-\theta)\,\gamma_{\mathrm{a}}\\
\quad +P_j^{\mathrm{AR}}(t,t_i)\,\Theta_j^{\mathrm{AR}}(t,t_i)\,(1-\theta),\\
P_j^{\mathrm{PR}}(t+1,t_i)=P_j^{\mathrm{AI}}(t,t_i)\,\gamma_{\mathrm{p}}\left(1-\Theta_j^{\mathrm{AI}}(t,t_i)+\Theta_j^{\mathrm{AI}}(t,t_i)\,\theta\right)\\
\quad +P_j^{\mathrm{PI}}(t,t_i)\,\gamma_{\mathrm{p}}\left(1-\Theta_j^{\mathrm{AI}}(t,t_i)+\Theta_j^{\mathrm{AI}}(t,t_i)\,\theta\right)\\
\quad +P_j^{\mathrm{AR}}(t,t_i)\left(1-\Theta_j^{\mathrm{AR}}(t,t_i)+\Theta_j^{\mathrm{AR}}(t,t_i)\,\theta\right)\\
\quad +P_j^{\mathrm{PR}}(t,t_i)\left(1-\tau_2+\tau_2\theta\right).
\end{cases} \tag{15}$$

The normalization condition

$$P_j^{\mathrm{AS}}(t,t_i)+P_j^{\mathrm{PS}}(t,t_i)+P_j^{\mathrm{AI}}(t,t_i)+P_j^{\mathrm{PI}}(t,t_i) \tag{16}$$

$$+P_j^{\mathrm{AR}}(t,t_i)+P_j^{\mathrm{PR}}(t,t_i)\equiv 1, \tag{17}$$

holds at any time step.

When t is sufficiently large, the probability of any state for any node reaches a steady state; thus, we have

$$\begin{cases}
P_j^{\mathrm{AS}}(t+1)=P_j^{\mathrm{AS}}(t)=P_j^{\mathrm{AS}},\\
P_j^{\mathrm{PS}}(t+1)=P_j^{\mathrm{PS}}(t)=P_j^{\mathrm{PS}},\\
P_j^{\mathrm{AI}}(t+1)=P_j^{\mathrm{AI}}(t)=P_j^{\mathrm{AI}},\\
P_j^{\mathrm{PI}}(t+1)=P_j^{\mathrm{PI}}(t)=P_j^{\mathrm{PI}},\\
P_j^{\mathrm{AR}}(t+1)=P_j^{\mathrm{AR}}(t)=P_j^{\mathrm{AR}},\\
P_j^{\mathrm{PR}}(t+1)=P_j^{\mathrm{PR}}(t)=P_j^{\mathrm{PR}}.
\end{cases} \tag{18}$$

Here, $P_i^{\mathrm{AS}}, P_i^{\mathrm{PS}}, P_i^{\mathrm{AI}}, P_i^{\mathrm{PI}}, P_i^{\mathrm{AR}}$, and P_i^{PR} represent the probabilities that individual i is in each of the six states when the system reaches the steady state.

As the infection rate β approaches the outbreak threshold β_{c} from below, the probability that nodes are infected on the epidemic spreading network tends to zero. In the steady state, the proportion of infected individuals in the system approaches zero, i.e.

$$P_{ij}^{\mathrm{I}}=\varepsilon_{ij}\ll 1. \tag{19}$$

The two infection probabilities of a node are defined as $P_{ij}^{\mathrm{AI}}=\varepsilon_{ij}^{\mathrm{A}}$ and $P_{ij}^{\mathrm{PI}}=\varepsilon_{ij}^{\mathrm{P}}$, so that

$$P_{ij}^{\mathrm{I}}=P_{ij}^{\mathrm{AI}}+P_{ij}^{\mathrm{PI}}=\varepsilon_{ij}^{\mathrm{A}}+\varepsilon_{ij}^{\mathrm{P}}. \tag{20}$$

From the definition, we obtain

$$\sum_k\sum_l b_{ijkl}\varepsilon_{kl}=\sum_k\sum_l b_{ijkl}\varepsilon_{kl}^{\mathrm{A}}+\sum_k\sum_l b_{ijkl}\varepsilon_{kl}^{\mathrm{P}}. \tag{21}$$

Dividing both sides of Eq. (21) by $\sum_k\sum_l b_{ijkl}\varepsilon_{kl}$ gives

$$1=\frac{\sum_k\sum_l b_{ijkl}\varepsilon_{kl}^{\mathrm{A}}}{\sum_k\sum_l b_{ijkl}\varepsilon_{kl}}+\frac{\sum_k\sum_l b_{ijkl}\varepsilon_{kl}^{\mathrm{P}}}{\sum_k\sum_l b_{ijkl}\varepsilon_{kl}}. \tag{22}$$

Define

$$f_{\mathrm{a}}=\frac{\sum_k\sum_l b_{ijkl}\varepsilon_{kl}^{\mathrm{A}}}{\sum_k\sum_l b_{ijkl}\varepsilon_{kl}},\quad f_{\mathrm{p}}=\frac{\sum_k\sum_l b_{ijkl}\varepsilon_{kl}^{\mathrm{P}}}{\sum_k\sum_l b_{ijkl}\varepsilon_{kl}}. \tag{23}$$

Neglecting higher-order terms, the last two terms of Eq. (13) can be approximated as

$$\begin{cases}
q_j^{\mathrm{AS}}(t,t_i)=\prod_k\prod_l\left[1-b_{ijkl}P_l^{\mathrm{AI}}(t,t_k)\omega_j(t,t_i)\alpha\beta\right]\\
\qquad\qquad \times\left[1-b_{ijkl}P_l^{\mathrm{PI}}(t,t_k)\omega_j(t,t_i)\alpha\varphi_1\beta\right]\\
\qquad\qquad \approx 1-\eta_{ij}(f_{\mathrm{a}}+\varphi_1 f_{\mathrm{p}}),\\
q_j^{\mathrm{PS}}(t,t_i)=\prod_k\prod_l\left[1-b_{ijkl}P_l^{\mathrm{AI}}(t,t_k)\omega_j(t,t_i)\varphi_2\alpha\beta\right]\\
\qquad\qquad \left[1-b_{ijkl}P_l^{\mathrm{PI}}(t,t_k)\omega_j(t,t_i)\varphi_2\alpha\varphi_1\beta\right]\\
\qquad\qquad \approx 1-\eta_{ij}(\varphi_2 f_{\mathrm{a}}+\varphi_1\varphi_2 f_{\mathrm{p}}),
\end{cases} \tag{24}$$

where

$$\eta_{ij}=\alpha\beta\,\omega_j(t,t_i)\sum_k\sum_l b_{ijkl}\varepsilon_{kl}. \tag{25}$$

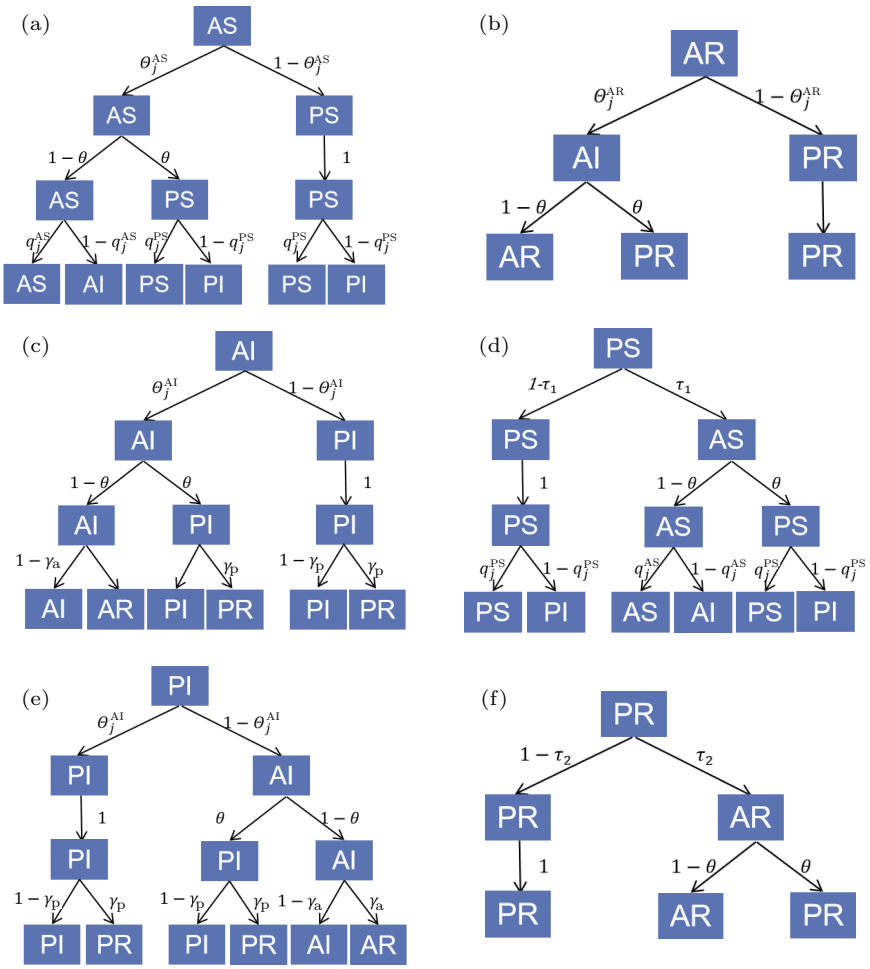


Fig. 3. The transition probability tree for the states of the APA-SIR dynamics in the multiplex networks per time step; each node has six possible states, including AS, PS, AI, PI, AR, and PR.

Near the steady state, $P_{ij}^{AI} \approx 0$, $P_{ij}^{PI} \approx 0$, so that $q_j^{AS}(t,t_i) \approx 1$ and $q_j^{PS}(t,t_i) \approx 1$. Substituting these approximations into the first two equations of Eq. (15), we obtain

$$\begin{cases} P_{ij}^{AS} = P_{ij}^{AS}\Theta^{AS}(1-\theta) + P_{ij}^{PS}\tau_1(1-\theta), \\ P_{ij}^{PS} = P_{ij}^{AS}(1-\Theta^{AS}+\Theta^{AS}\theta) + P_{ij}^{PS}(1-\tau_1+\tau_1\theta). \end{cases} \tag{26}$$

Substituting Eq. (26) into the third and fourth equations of Eq. (15), the probability that the i-th batch, j-th node is infected is

$$\begin{aligned} \varepsilon_{ij} &= P_{ij}^{AS}(1-q^{AS}) + P_{ij}^{PS}(1-q^{PS}) \\ &\quad + \varepsilon_{ij}\left[1-(1-\xi)(\Theta^{AI}-\theta\Theta^{AI})\gamma_p\right]. \end{aligned} \tag{27}$$

Defining $A = (1-\xi)(\Theta^{AI}-\theta\Theta^{AI})\gamma_p$, Eq. (27) can be simplified as

$$\begin{aligned} A\varepsilon_{ij} &= P_{ij}^{AS}(1-q^{AS}) + P_{ij}^{PS}(1-q^{PS}) \\ &= \eta_{ij}\left[P_{ij}^{AS}(f_a+\varphi_1 f_p) + P_{ij}^{PS}(\varphi_2 f_a + \varphi_1\varphi_2 f_p)\right]. \end{aligned} \tag{28}$$

Summing over all neighbors and rearranging gives

$$\begin{aligned} \sum_{kl}\Big\{ &\left[P_{ij}^{AS}(f_a+\varphi_1 f_p) + P_{ij}^{PS}(\varphi_2 f_a+\varphi_1\varphi_2 f_p)\right] \\ &\times\alpha\omega_j(t,t_i)b_{ijkl} - \frac{A}{\beta}c_{ijkl}\Big\}\varepsilon_{kl} = 0, \end{aligned} \tag{29}$$

where c_{ijkl} is the element of the identity matrix, $c_{ijkl} = 1$ if $ij = kl$, and 0 otherwise. Let $\boldsymbol{F}$ be the matrix with elements

$$\begin{aligned} f_{ijkl} &= \alpha\omega_j(t,t_i)b_{ijkl}\left[P_{ij}^{AS}(f_a+\varphi_1 f_p)\right. \\ &\quad \left. + P_{ij}^{PS}(\varphi_2 f_a + \varphi_1\varphi_2 f_p)\right]. \end{aligned} \tag{30}$$

Then, the epidemic outbreak threshold of the model can be expressed as

$$\beta_c = \frac{A}{\Lambda_{\max}(\boldsymbol{F})}, \tag{31}$$

where $\Lambda_{\max}(\boldsymbol{F})$ is the largest eigenvalue of $\boldsymbol{F}$.

This relationship indicates that the epidemic outbreak threshold is closely related to the spread of awareness in the upper-layer network. Other factors, such as susceptibility, virus transmission rate, influence factor, mass media conversion rate, and recovery rate γ_p of strongly aware infectors, also affect the threshold.

4. Numerical simulation

In this section, we conduct extensive simulations to analyze the proposed M-APA-SIR model, revealing the effects

of different factors on the coupled dynamic network and validating the accuracy of the MMCA through Monte Carlo (MC) simulations. The SIR model adopted in this study assumes that recovered individuals cannot be reinfected. At the steady state, the recovered proportion (ρ^{R}) represents the total infection proportion, i.e., the final epidemic size. Therefore, our numerical simulations and analysis primarily focus on the steady-state value of ρ^{R} to investigate the epidemic's evolution characteristics.

Using the MMCA framework, we sequentially examine the impact of various parameters on the proportion of strongly aware individuals (ρ^{P}), recovered individuals in the epidemic (ρ^{R}), and infected individuals (ρ^{I}). The simulation results confirm the accuracy of the theoretical analysis and provide insights for effective epidemic control.

Table 2. Hyperetwork parameters for initial settings.

Hypernetwork parameters	Parametrization	Value
The social layer has a hyperedge to select the number of nodes	u_1	uniform distribution on (15,25)
Physical contact layer a hyperedge selection node number	u_2	uniform distribution on (3,25)
Disease pain level	v	0.2
The average severity of symptoms experienced by the infected person	μ	0.15
The variance of the severity of symptoms experienced by the infected person	σ^2	0.1
Information acceptance rate	λ	0.4
Influence factor of information reception rate under weak awareness state	ω_1	1
Influence factor of information reception rate under strong awareness state	ω_2	2
Probability of transition from strong to weak awareness in susceptible individuals	τ_1	0.2
Probability of transition from strong to weak awareness in recovery individuals	τ_2	0.1
Official media coverage rate	M	0.6
Probability of transitioning to a strong awareness state under the influence of mass media	θ	0.2
Susceptibility rate	α	0.4
Virus transmission rate	β	0.6
The mean recovery rate of highly conscious infected individuals	μ_1	0.4
The variance of the recovery rate of highly conscious infected individuals	σ_1^2	0.2

In the simulations, the initial number of nodes N_0 in each layer of the network is set to 35. Following the hypernetwork evolution process, an initial social network of $N = 1000$ nodes is randomly generated. The initial fractions of individuals in the epidemic and awareness states are set as $P^{\mathrm{P}}(0) = 0.01$ and $P^{\mathrm{I}}(0) = 0.01$, respectively.

The group unit of information dissemination in each hyperedge is modeled as an "information-sharing group" consisting of 15 to 25 individuals, in line with Dunbar's number[28] and diffusion theory.[29] This ensures high-frequency interactions, strong potential for diffusion, and close interpersonal connections. Information within these groups is easily shared and less likely to be ignored, while heterogeneity among members promotes deeper diffusion. Consequently, the number of nodes per hyperedge in the information propagation layer, denoted as μ_1, is set to $U(15\text{–}25)$.

According to information overload (IO)[30] and bounded rationality (BR) theories,[31] individuals in modern society are frequently exposed to excessive or conflicting health information, which often leads to reduced information reception via a "filtering mechanism." The limited information processing capacity imposed by BR causes individuals to prioritize information related to personal interests (e.g., work, family) while being selective about health information. Simplifying these effects of IO and BR, the information acceptance rate is set to $\lambda = 0.4$. The initial values for other model parameters are summarized in Table 2.[17,22,32,33]

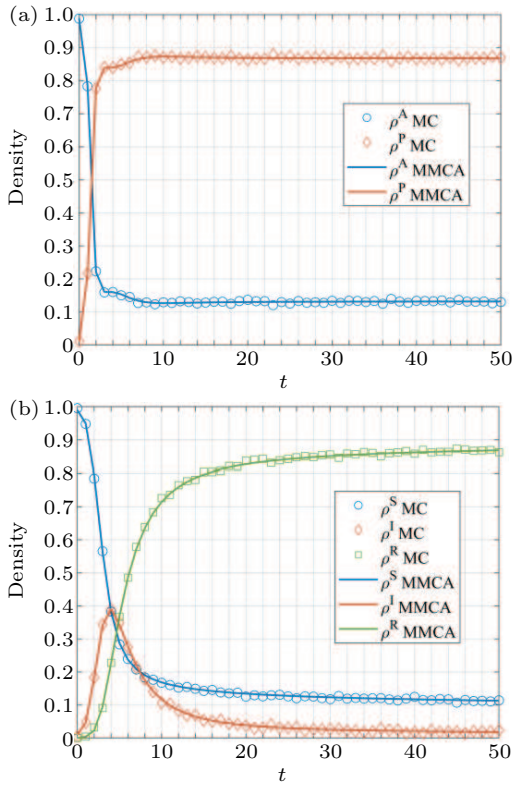


Fig. 4. Comparison of the simulation results between MC and MMCA for the M-APA-SIR model, showing the temporal evolution of the proportion of individuals in each state over time step t.

First, Fig. 4 illustrates the temporal variations in the proportions of different states over time t, where line graphs represent the MMCA results and dot plots correspond to MC simulation outcomes. Figure 4(a) shows the evolution of individuals in the weak awareness state (ρ^{A}) and the strong awareness state (ρ^{P}) during information dissemination. Figure 4(b) depicts the changes in the proportions of susceptible (ρ^{S}), infected (ρ^{I}), and recovered (ρ^{R}) individuals during the spread of the infectious disease. The figures indicate that the MMCA results are in close agreement with the MC simulations. Therefore, all subsequent numerical experiments in this study are conducted using MMCA for efficiency.

4.1. Impact of influence factors φ_1 and φ_2 on the epidemic size ρ^{R}

Figure 5 illustrates the combined effects of susceptibility α and transmission rate β on epidemic propagation. Here, α represents an individual's susceptibility to viral infection, with higher values indicating greater susceptibility, while β denotes the probability of infection per contact. The results show that increases in either parameter lead to a significant rise in the proportion of infected individuals, facilitating epidemic spread. Conversely, reducing individual susceptibility or limiting transmission pathways can effectively mitigate epidemic propagation. The interaction between α and β highlights a critical threshold at which the dynamics shift from containment to widespread outbreak, underscoring the importance of controlling these parameters to suppress epidemic transmission.

Next, we conducted a detailed analysis of the influence coefficients φ_1 and φ_2, which characterize the effects of consciousness states on susceptibility α and transmission rate β, respectively, and their impact on the epidemic size ρ^{R}. Here, φ_1 represents the reduced probability that susceptible individuals with heightened awareness become infected, whereas φ_2 indicates the decreased transmission rate among infectious individuals with heightened awareness.

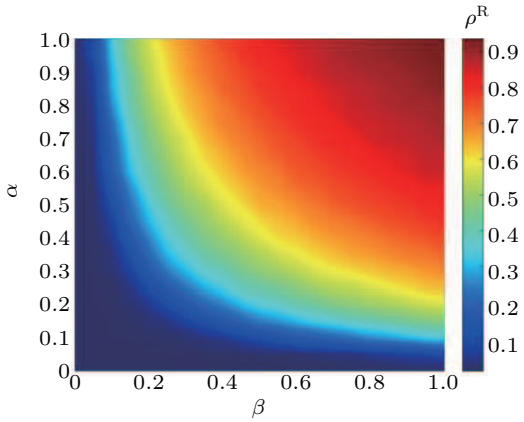


Fig. 5. Combined effects of susceptibility rate α and transmission rate β on epidemic spread. Other parameters are set as follows: $\tau_1 = 0.3$, $\tau_2 = 0.2$, $M = 0.4$, $\varphi_1 = 0.4$, and $\varphi_2 = 0.4$.

As shown in Figs. 6(a)–6(c), increasing φ_1 from 0.2 to 0.8 significantly accelerates the transition of individuals from the S state to the R state. The rapid dissemination of epidemic-related information enhances public attention, prompting individuals to adopt appropriate preventive measures and partially suppressing disease spread. This mechanism underscores the critical role of information propagation during public health crises and highlights its importance in controlling epidemic escalation.

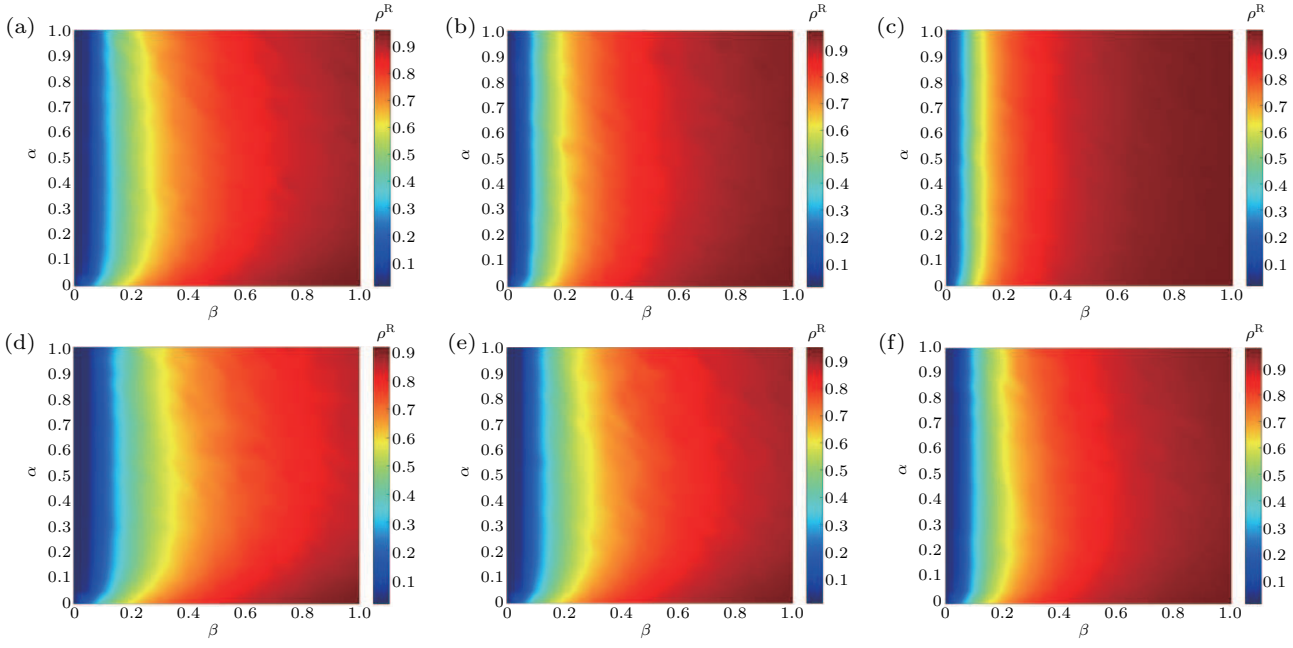


Fig. 6. Relationship between the steady-state proportion of recovered individuals (ρ^{R}) and the opinion acceptance rate, as well as the virus transmission rate, under different magnitudes of influence factors φ_1 and φ_2. In (a)–(c), φ_2 is fixed at 0.5. In (d)–(f), φ_1 is fixed at 0.2. Other parameters for all insets are set as: $\tau_1 = 0.3$, $\tau_2 = 0.2$, and $\mu_1 = 0.8$.

From Figs. 6(d)–6(f), it is also evident that the parameter φ_2 has a significant effect on the final epidemic size. Smaller values of φ_2 indicate that infectious individuals with strong awareness take protective actions, such as self-isolation, thereby reducing the likelihood of secondary infections. Consequently, when individuals' protective behaviors are strongly influenced by positive information, the collective advantage in epidemic control becomes pronounced.

Furthermore, as shown in Fig. 6, the impact of the information reception parameter λ on the steady-state proportion of recovered individuals (ρ^{R}) gradually diminishes as φ_1 and φ_2 increase. This occurs because a larger proportion of individuals with a comprehensive understanding of the epidemic enhances public awareness of preventive measures, reducing disease transmission and controlling outbreak scale. This phenomenon demonstrates that thorough public understanding of the epidemic can improve preventive awareness and effectively inhibit virus spread.

These findings suggest that governments should strengthen information disclosure and science popularization, providing accurate, timely, and comprehensive epidemic information to enhance public understanding and response capability. Encouraging proactive preventive behaviors, disseminating health knowledge through multiple channels, reducing rumor propagation, and promoting social cooperation collectively contribute to effective epidemic control.

4.2. The influence of epidemic pain degree v

Figure 7 illustrates the combined impact of the virus transmission rate (β) and disease pain perception (v) on the proportion of recovered individuals (ρ^{R}). In infectious disease dynamics, the recovered proportion is closely linked to the infected proportion, as individuals typically transition to the recovered state after a period of infection and treatment.

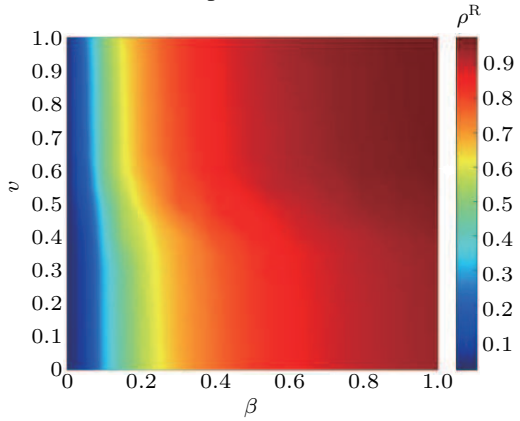


Fig. 7. Phase diagram showing the density of recovered individuals (ρ^{R}) under varying infection rates (β) and epidemic pain levels (v). The other parameters are set as: $\mu = 0.6$, $\tau_1 = 0.3$, $\tau_2 = 0.2$, and $\mu_1 = 0.8$.

From the figure, it is evident that as both β and v increase, the recovery proportion rises significantly. Specifically, when β is low (e.g., 0.1–0.3) and v is high (close to 1), ρ^{R} can reach 0.6–0.8. This occurs because highly sensitive individuals (high v) detect symptoms early, adopt effective preventive measures, and thus promote recovery. In contrast, when v is low (close to 0), infected individuals are less aware of symptoms, resulting in a lower recovery proportion (around 0.2–0.4), even if the virus transmission rate is modest.

As both β and v increase further, the recovery proportion improves substantially. When v exceeds 0.4, indicating that individuals are more sensitive to disease discomfort, ρ^{R} may approach 0.9. This suggests that heightened symptom awareness transforms into proactive behavior, encouraging individuals to cooperate with treatment and increasing recovery likelihood. Moreover, when $\beta > 0.5$ (faster transmission) and v is high, the recovery proportion remains elevated.

These observations highlight the crucial role of individual perception and cognition of disease in controlling epidemic spread and promoting recovery.

4.3. The influence of mass media mapping quantity M

Figure 8(a) shows the spatial distribution of public awareness of infectious disease prevention under varying virus transmission rates (β) and the extent of official media coverage (M). As β increases, public awareness of disease prevention gradually strengthens, indicating that higher transmission rates motivate more attention to infectious diseases, likely due to information diffusion and heightened social concern. When β exceeds approximately 0.2, further increases in β have a diminishing effect on the proportion of strongly aware individuals (ρ^{P}), whereas expanding media coverage continues to boost awareness. For instance, when media coverage is low (around 0.2), average public awareness is about 0.76; increasing coverage to nearly 1.0 raises awareness to roughly 0.89, demonstrating that broader media dissemination can increase public awareness by approximately 0.13. This highlights the critical role of official media in enhancing societal awareness and supporting epidemic mitigation.

Figure 8(b) illustrates the effect of β and M on the recovery proportion (ρ^{R}). As β increases, ρ^{R} generally rises, reflecting more individuals becoming infected and subsequently recovering. Higher values of M further improve recovery rates, suggesting that widespread dissemination of official information promotes public adherence to preventive measures and treatment guidelines. Conversely, regions with both low β and low M exhibit lower recovery proportions, indicating that limited viral spread coupled with insufficient media coverage hampers effective recovery. These results underscore the importance of managing both viral transmission and the reach of information campaigns to enhance epidemic control and recovery outcomes, providing actionable insights for optimizing public health interventions.

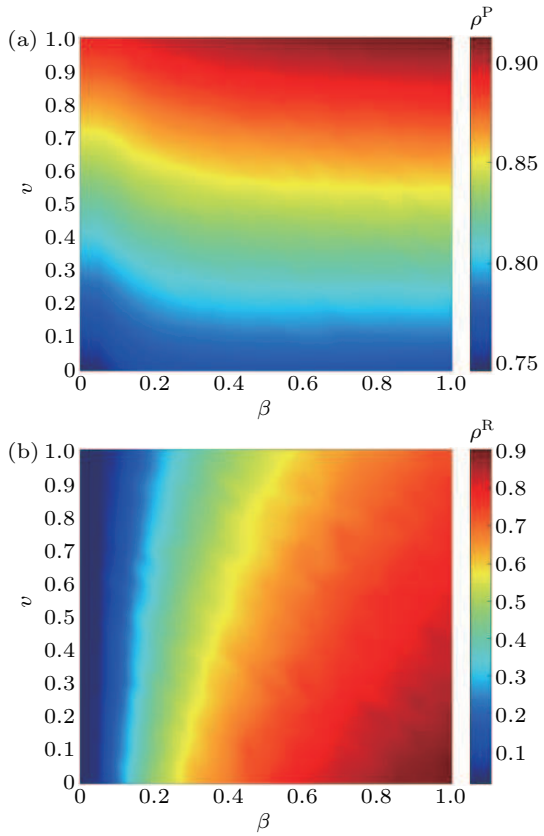


Fig. 8. Density of strongly aware individuals and recovered individuals under varying infection rate (β) and mass media coverage rate (M) in full phase diagrams. In (a), the fraction of strongly aware individuals (ρ^{P}) is shown through MMCA analysis as a function of β and M at the stationary state on different multiplex networks. In (b), the fraction of recovered individuals (ρ^{R}) is shown through MMCA analysis as a function of β and M at the stationary state on different multiplex networks. Other parameters for each inset are: $\tau_1 = 0.3$, $\tau_2 = 0.2$, $\mu_1 = 0.8$, $\theta = 0.6$.

4.4. The influence of patient recovery rate μ_1 and epidemic pain degree

Finally, we investigate the effects of different values of μ_1 and epidemic pain degree v on the peak infection ratio ρ^{I} and its steady-state value. The parameter μ_1 represents the average natural recovery rate of highly aware infected individuals.

Figure 9 shows that, regardless of the value of v, higher values of μ_1 result in a smaller final proportion of infected individuals. When the recovery rate is high ($\mu_1 > 0.4$), the infection ratio ρ^{I} declines rapidly and eventually converges to zero. This indicates that increasing μ_1 enhances the mitigating effect of highly aware individuals on epidemic spread, thereby reducing the final outbreak size. This finding underscores the crucial role of recovery speed in epidemic control: by improving individuals' recovery capacity, the transmission chain can be rapidly interrupted, effectively suppressing disease spread.

From Fig. 9, it is also observed that as v increases from 0.3 to 0.8, the peak infection ratio significantly rises. Moreover, when $\mu_1 = 0.4$, the time for the infection proportion to decline to zero is delayed from around 22 to approximately 26 as v increases. This suggests that higher pain perception accelerates the transition of individuals from a strongly aware to a weakened state, and individuals in the weakened state exhibit higher infection rates. Meanwhile, the slower recovery of weakened infected individuals prolongs their presence in the high-infection-rate state, delaying the decline of ρ^{I} to zero and further facilitating epidemic spread.

These results suggest that controlling the level of pain and improving the overall recovery efficiency of the population are crucial strategies for reducing the infection peak and the duration of the epidemic. The government should adopt multiple measures: on one hand, alleviate the pain and discomfort of the infected individuals by providing medication and psychological support, which can slow down the transition from a strong to a weakened state and reduce the number of individuals in a weakened state with high infection rates; on the other hand, increase medical resources, especially rehabilitation services, to enhance the overall recovery efficiency of the population and shorten the duration of time spent in a high-risk infection state. At the same time, early diagnosis and timely treatment should be strengthened to help infected individuals recover as soon as possible, reducing the spread of the virus. Additionally, strict isolation and prevention measures should be implemented, especially for those in weakened states, limiting their contact with others to block the transmission chain. Public health education should also be enhanced to raise awareness of preventive measures and advocate for necessary protective actions. By reducing the infection peak and shortening the duration of the epidemic, effective control of the epidemic can be achieved.

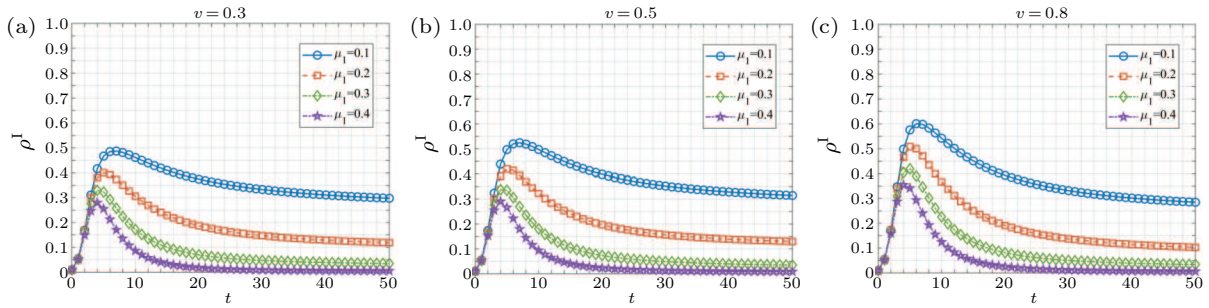


Fig. 9. The proportion of individuals in the infected state (ρ^{I}) as a function of time step t, under different average recovery rates (μ_1) and disease pain levels (v). The other parameters for each inset are set as: $\mu = 0.4$, $\lambda = 0.8$, $\tau_1 = 0.3$, $\tau_2 = 0.2$, $\alpha = 0.8$.

5. Conclusion

The outbreak of infectious disease information is usually accompanied by the rapid spread of the disease, with increasing attention to the epidemic from various sectors of society. During this rapid information dissemination, the public's awareness and behavior regarding disease prevention will also respond quickly. Different individuals, based on their health status, social environment, and the information received, make corresponding response decisions. This study is based on a three-layer network epidemic model (public media layer — information layer — epidemic layer) of hypergraphs, incorporating individual heterogeneity and higher-order group interaction effects. The model includes the variation in individual awareness influenced by their own health status, and the changes in individual awareness responses. It also embeds dual influence factors to regulate the awareness dependency of infection and transmission probabilities. Subsequently, we analyzed the proposed model using the MMCA theory and validated the accuracy of MMCA through Monte Carlo numerical simulations.

Next, we analyze the impact of key dynamic and structural parameters on the proposed coupled media-awareness-epidemic dynamics. Previous studies mainly focused on how the prevention awareness of susceptible individuals affects their infection probability, but ignored the impact of the prevention awareness of infected individuals on the transmission rate.[11,15,34] We expanded our analysis to explore the interaction among preventive awareness, the transmission ability of infected individuals, and the sensitivity of susceptible individuals to the virus. The media coverage rate, a factor often overlooked in previous studies,[12,22,35,36] was simulated to examine how these factors affect the scale and duration of the epidemic. The results indicate that susceptibility and transmission rate are important factors influencing the scale of the epidemic outbreak. Official media reports with high coverage timely convey accurate information and effectively curb the spread of rumors. Controlling the level of pain and improving the overall recovery efficiency of the population are important strategies to reduce the infection peak and the duration of the epidemic.

The research offers meaningful guidance for epidemic prevention and control, helping individuals to adopt appropriate measures and understand the role of awareness dissemination in real-world epidemic control scenarios. The limitation of this study lies in the lack of actual data on information dissemination. In addition, there are still differences from the real model. In the future, data such as climate, transportation, and business will be combined to improve the model's predictive ability. Meanwhile, we will conduct in-depth research on the impact of offline interaction among urban individuals,[37] community structure, community centers,[38] urban population density,[39] and urbanization process[40] on information and the spread of the epidemic, to enhance the practicality and predictive level of the model. These will become the key directions in the future.

Acknowledgment

Project supported by the Fundamental Research Funds for the Central Universities (Grant No. N2406015).

References

[1] Kiss I Z, Cassell J, Recker M and Simon P L 2010 *Math. Biosci.* **225** 1
[2] Liu X, Zheng L, Jia X, Qi H, Yu S and Wang X 2021 *IEEE Trans. Comput. Soc. Syst.* **8** 1042
[3] Li L, Zhang Q, Wang X, Zhang J, Wang T, Gao T L, Duan W, Tsoi K K and Wang F Y 2020 *IEEE Trans. Comput. Soc. Syst.* **7** 556
[4] Chu D K, Akl E A, Duda S, *et al.* 2020 *Lancet* **395** 1973
[5] Stockmaier S, Stroeymeyt N, Shattuck E C, Hawley D M, Meyers L A and Bolnick D I 2021 *Science* **371** eabc8881
[6] Li B and Zhu L 2024 *Inf. Process. Manage.* **61** 103621
[7] Yuan T, Guan G, Shen S and Zhu L 2023 *J. Math. Anal. Appl.* **526** 127273
[8] Sha H and Zhu L 2025 *Inf. Process. Manage.* **62** 104016
[9] Granell C, Gomez S and Arenas A 2013 *Phys. Rev. Lett.* **111** 128701
[10] Granell C, Gomez S and Arenas A 2014 *Phys. Rev. E* **90** 012808
[11] Xia C, Wang Z, Zheng C, Guo Q, Shi Y, Dehmer M and Chen Z 2019 *Inf. Sci.* **471** 185
[12] Sun M, Tao Y and Fu X 2021 *Chaos* **31** 093134
[13] Fang F, Ma J and Li Y 2023 *Chaos, Solitons & Fractals* **170** 113376
[14] Han D and Wang X 2024 *Chaos, Solitons & Fractals* **186** 115264
[15] Yu Y and Huo L 2025 *Appl. Math. Comput.* **499** 129406
[16] Huo L and Yin L 2025 *Chin. Phys. B* **34** 68902
[17] Xu J, Li J, Han Z and Zhu P 2024 *Chaos, Solitons & Fractals* **187** 115335
[18] Wang J W, Rong L L, Deng Q H and Zhang J Y 2010 *Eur. Phys. J. B* **77** 493
[19] Suo Q, Guo J L, Sun S and Liu H 2018 *Physica A* **489** 141
[20] Wang Z, Yin H and Jiang X 2020 *Physica A* **544** 122545
[21] Sun Y, Wang P, Wang Y and Wang Z 2023 *Int. J. Innov. Comput. Inf. Control* **19** 687
[22] Xie S, Wang P, Wang Z and Zheng Y 2025 *IInt. J. Innov. Comput. Inf. Control* **21** 617
[23] Berge C 1973 *Graphs and Hypergraphs* (Amsterdam: North-Holland Publishing Company)
[24] Berge C 1989 *Hypergraphs: Combinatorics of Finite Sets* (Amsterdam: North-Holland Publishing Company)
[25] Estrada E and Rodríguez-Velázquez J A 2006 *Physica A* **364** 581
[26] Shen A Z, Guo J L and Suo Q 2017 *Chaos, Solitons & Fractals* **97** 84
[27] GShen A Z, Guo J L, Wu G L, *et al.* 2018 *Chaos, Solitons & Fractals* **114** 461
[28] Dunbar R I M 1992 *J. Hum. Evol.* **22** 469
[29] Rogers E M 2003 *Diffusion of Innovations* (New York: Free Press)
[30] Kashada A, Isnoun A and Aldali N 2020 *Int. J. Latest Eng. Res. Appl.* **5** 53
[31] Simon H A 1957 *Models of Man; Social and Rational* (Oxford: Wiley)
[32] Zhang J and Wang N 2024 *Expert Syst. Appl.* **249** 123725
[33] Fang F, Ma J and Li Y 2023 *Chaos, Solitons & Fractals* **170** 113376
[34] Liu Y, Xiao W, Qiu X and Wang J 2025 *Phys. Lett. A* **545** 130494
[35] Huo L and Yu Y 2023 *Chin. Phys. B* **32** 108703
[36] Yu Y and Huo L 2025 *Inf. Sci.* **689** 121414
[37] Liu C, Yang Y, Chen B, Cui T, Shang F, Fan J and Li R 2022 *Chaos* **32** 081105
[38] Shi D, Shang F, Chen B, Expert P, Lü L, Stanley H E, Lambiotte R, Evans T S and Li R 2024 *Commun. Phys.* **7** 170
[39] Li R, Richmond P and Roehner B M 2018 *Physica A* **510** 713
[40] Li R, Dong L, Zhang J, Wang X, Wang W X, Di Z and Stanley H E 2017 *Nat. Commun.* **8** 1841